Hindawi
Journal of Nanomaterials
Volume 2020, Article ID 8276745, 16 pages
https://doi.org/10.1155/2020/8276745

Research Article

A Thermodynamics-Based Nonlocal Bar-Elastic Substrate Model with Inclusion of Surface-Energy Effect

Worathep Sae-Long,[1] Suchart Limkatanyu,[1] Woraphot Prachasaree,[1] Jaroon Rungamornrat,[2] and Piti Sukontasukkul[3]

[1]*Department of Civil Engineering, Faculty of Engineering, Prince of Songkla University, Songkhla 90112, Thailand*
[2]*Applied Mechanics and Structures Research Unit, Department of Civil Engineering, Faculty of Engineering, Chulalongkorn University, Bangkok 10330, Thailand*
[3]*Construction and Building Materials Research Center, Department of Civil Engineering, King Mongkut's University of Technology North Bangkok, Bangkok 10800, Thailand*

Correspondence should be addressed to Suchart Limkatanyu; suchart.l@psu.ac.th

Received 19 December 2019; Revised 14 February 2020; Accepted 21 April 2020; Published 16 May 2020

Academic Editor: Francesco Marotti de Sciarra

This paper presents a bar-elastic substrate model to investigate the axial responses of nanowire-elastic substrate systems considering the effects of nonlocality and surface energy. The thermodynamics-based strain gradient model is adopted to capture the nonlocality of the bar-bulk material while the Gurtin-Murdoch surface theory is utilized to consider the surface energy. To characterize the bar-surrounding substrate interaction, the Winkler foundation model is employed. In a direct manner, system compatibility conditions are obtained while within the framework of the virtual displacement principle, the system equilibrium condition and the corresponding natural boundary conditions are consistently obtained. Three numerical simulations are conducted to investigate the characteristics and behaviors of the nanowire-elastic substrate system: the first is conducted to reveal the capability of the proposed model to eliminate the paradoxical behavior inherent to the Eringen nonlocal differential model; the second is employed to characterize responses of the nanowire-elastic substrate system; and the third is aimed at demonstrating the dependence of the system effective Young's modulus on several system parameters.

1. Introduction

Nowadays, nanotechnology and nanoscience are at the front line of modern research and play a crucial role in developing novel devices and systems at nanoscale. Such devices and systems are found to have a broad spectrum of modern applications in engineering and science such as bionanoactuators, nanosensors, nanowires, nanoprobes, and graphene sheets [1–6]. Usually, structural members (bar, beam, plate, and shell) are integrated as components of such devices and systems [7]. Therefore, understanding and characterizing structural behaviors at a nanoscale are deemed essential in designing these devices and systems. Both experimental and analytical research works have been conducted on nanostructures by researchers worldwide. Nonetheless, it is usually difficult and expensive to carry out experimental work on such tiny structures while atomistic computational models [8–10] generally demand high computational cost in nanostructure modelling. Therefore, researchers worldwide have sought for alternative approaches to characterize the structural behaviors at nanoscale. As an excellent alternative, structural models are able to balance model validity and model effectiveness, and their formulations are generally based on mechanics-of-materials theories ranging from comparatively simple bar theory to a sophisticated curvilinear shell theory. However, conventional structural models fail to characterize some intrinsic features of nano-sized structures, namely small-scale effect and size-dependent effect. These two effects influence elastic property as well as responses of nano-sized structures as confirmed by experiments and

atomistic simulations [11–13]. In general, it is well accepted that the long-range interatomic interaction induces the small-scale effect while energy associated with atoms at the free surface causes the size-dependent effect. Several structural models have been armed with the ability to account for these two effects. This has been achieved by incorporating nonclassical continuum-mechanics theory and surface elasticity theory into conventional structural models.

The effect of long-range interatomic interaction becomes more pronounced and is increasingly required to be taken into account when the dimension of a structure is in the order of nanometer. The discrete nature of materials is responsible for this effect. To account for the discrete nature of materials, researchers have proposed several enhanced continuum-mechanics theories [14–18]. The most popular one is the Eringen differential form of the strain-driven nonlocal elasticity model [15, 16]. A countless list of structural-mechanics models have been cooperated with this nonlocal differential model [19–22]. As one of the earliest research works on the application of the Eringen nonlocal differential model, Peddieson et al. [19] investigated flexural responses of nanobeams under different support systems and various loading types using the nonlocal Euler-Bernoulli beam model. However, there is no nonlocal effect detected by this nonlocal beam model for the case of a cantilever nanobeam subjected to end force. Peddieson et al. [19] called this peculiar response a "paradox" without any diagnosis. Romano et al. [23] have recently diagnosed the cause of this paradox and showed that the paradoxical response inherent to the Eringen nonlocal differential model is associated with the ill-posedness of Eringen's nonlocal differential model in structural-mechanics problems. Various forms of improved nonlocal constitutive models have been invented and employed by several researchers to remedy this paradoxical response, thus resulting in a well-posed nonlocal structural problem [24–26], for example, the stress-driven integral nonlocal constitutive model proposed by Romano and Barretta [24], the thermodynamics-based strain gradient model proposed by Barretta and Marotti de Sciarra [25], and the nonlocal strain gradient model proposed by Barretta and Marotti de Sciarra [26]. Among these improved nonlocal constitutive models, the thermodynamics-based strain gradient model proposed by Barretta and Marotti de Sciarra [25] is of particular interest in the present study since it can be implemented with reasonable effort. It is worth mentioning that nanobeams based on the thermodynamics-based strain gradient model show no paradoxical response.

As the dimension of a structure approaches a nanoscale range, energy corresponding to atoms at the free surface varies from that associated with the atoms in the core-bulk material, thus resulting in an excess of energy corresponding to the surface atoms. In nano-sized structures, this excess energy-known as "surface free energy" becomes sizable when compared to the bulk energy due to a large surface-to-volume ratio. The surface elasticity theory was first proposed by Gurtin and Murdoch [27, 28]. To include the surface-energy effect, this theory has been integrated with the classical continuum-mechanics model. Several structural models (bar, beam, and plate) have employed the Gurtin-Murdoch surface elasticity model [29–33].

As a common type of nanostructure, a wide range of applications have been found for nanowires, and they cover biosensors, optoelectronics, biotechnology, and micro/nanoelectromechanical systems (M/NEMS) [3, 34, 35]. In nanodevices, elastic substrate media have often been used to integrate nanowires into larger parts. Consequently, the nanowire-surrounding substrate interaction plays an essential role in controlling the response of those nanodevices. In literatures, various nanowire-elastic substrate models have been proposed to investigate the responses of nanowire-elastic substrate systems (bending, buckling, and vibration). For example, static bending responses of silver nanowire-elastic substrate systems were analytically investigated by Khajeansari et al. [36]; buckling loads of nanowire-elastic substrate systems were analytically determined by Zhao et al. [37]; effects of nonlocality and surface energy on vibrating responses of nanowire-elastic substrate systems were studied by Malekzadeh and Shojaee [38] using beam theories.

In the present study, the main focus is on the behavior of nanobar-elastic substrate systems under tensile loadings. Up to date, only few numerical models have been proposed to investigate the tensile behavior of nanobar-elastic substrate systems [31, 39] and the "paradoxical" Eringen nonlocal differential model has been incorporated into those models. Therefore, there is still room to propose a "*paradox-free*" nanobar-elastic substrate medium model for the research community. The general idea and framework of the proposed model follow the nanobar-elastic substrate medium model proposed by Limkatanyu et al. [31] but the "paradox-free" thermodynamics-based strain gradient constitutive law [25] is employed to account for the nonlocality of the bar-bulk material, thus resulting a more rational nanobar-elastic substrate medium model.

Organization of the present work is as follows: brief introductions to thermodynamics-based strain gradient model and surface elasticity model are first described. The former is employed to account for small-scale effect while the latter is used to include the size-dependent effect. A complete set of basic equations (compatibility conditions, equilibrium equation, and sectional constitutive relation) are then derived for the nanobar-elastic substrate system. To study the characteristics and behaviors of the nanowire-elastic substrate system, three numerical simulations employing the proposed model are finally conducted: the first considering only the small-scale effect is employed to present the capability of the proposed model to eliminate the paradoxical response associated with the Eringen nonlocal differential model; the second is employed to characterize responses of the nanowire-elastic substrate system; and the third is employed to demonstrate the dependence of the system effective Young's modulus on several system parameters.

2. Nanobars with Small-Scale and Size-Dependent Effects

The present work employs two nonclassical elasticity models: the thermodynamics-based strain gradient model and the surface elasticity model to take into account the unique characteristics intrinsic to nano-sized structures.

Brief introductions of these two nonclassical elasticity models are given as follows.

2.1. Thermodynamics-Based Strain Gradient Model. Unlike classical elasticity model, the thermodynamics-based strain gradient model defines the stress field at a generic point as a function of both the strain and the strain gradient at that particular point to account for higher-order deformation mechanism present in nano-sized structures [40]. The original form of the strain gradient model dates back to the model proposed by Mindlin [41] and contains 18 independent material constants for an isotropic homogeneous elastic body, thus causing difficulty in determination and calibration of those material constants. A modified version of the strain gradient model was subsequently proposed by Altan and Aifantis [42] and contains only one single material constant, thus simplifying the material-constant determination and calibration. The present work employs this modified strain gradient model formulated within the framework of thermodynamics by Barretta and Marotti de Sciarra [25] to represent the nonlocality of the bar-bulk material.

For a uniaxial response, the strain energy density functional of the strain gradient material is given by Barretta and Marotti de Sciarra [25] as

$$\Psi\left[\varepsilon_{xx}(x), \varepsilon_{xx}^{\nabla}(x)\right] = \frac{1}{2}E_{xx}\varepsilon_{xx}^{2}(x) + \frac{1}{2}(e_0 a)^2 E_{xx}\left(\varepsilon_{xx}^{\nabla}(x)\right)^2, \quad (1)$$

where E_{xx} defines the Young modulus, $\varepsilon_{xx}(x)$ the axial strain, $\varepsilon_{xx}^{\nabla}(x) = \partial\varepsilon_{xx}(x)/\partial x$ the axial strain gradient, e_0 the material constant which can be determined approximately or experimentally, and a the internal characteristic length. The rate form (time derivative) of the strain energy density functional Ψ is

$$\dot{\Psi}\left[\varepsilon_{xx}(x), \varepsilon_{xx}^{\nabla}(x)\right] = \frac{\partial\Psi}{\partial\varepsilon_{xx}}\dot{\varepsilon}_{xx} + \frac{\partial\Psi}{\partial\varepsilon_{xx}^{\nabla}}\dot{\varepsilon}_{xx}^{\nabla} = \sigma_{xx}^{0}\dot{\varepsilon}_{xx} + \sigma_{xx}^{1}\dot{\varepsilon}_{xx}^{\nabla}, \quad (2)$$

with a dot $(\dot{\ })$ representing the time derivative and σ_{xx}^{0} and σ_{xx}^{1} being defined as

$$\sigma_{xx}^{0} = \frac{\partial\Psi}{\partial\varepsilon_{xx}} = E_{xx}\varepsilon_{xx},$$
$$\sigma_{xx}^{1} = \frac{\partial\Psi}{\partial\varepsilon_{xx}^{\nabla}} = (e_0 a)^2 E_{xx}\varepsilon_{xx}^{\nabla}. \quad (3)$$

From the energy (work) point of view, Equation (3) clearly indicates that σ_{xx}^{0} represents the local (conventional) axial stress and is the conjugate-work pair of the axial strain $\varepsilon_{xx}(x)$ while σ_{xx}^{1} represents the higher-order axial stress and is the conjugate-work pair of the axial strain gradient $\varepsilon_{xx}^{\nabla}(x)$. To satisfy the thermodynamic condition, Equation (2) is put into the framework of thermodynamics represented in Equation (4):

$$\int_L\left(\int_A \sigma_{xx}\dot{\varepsilon}_{xx}dA\right)dx - \int_L\left(\int_A \dot{\Psi}dA\right)dx = 0, \quad (4)$$

where σ_{xx} is the nonlocal axial stress. Substituting Equation (2) into Equation (4) yields the following expression:

$$\int_L\left(\int_A \sigma_{xx}dA\right)\dot{\varepsilon}_{xx}\,dx - \int_L\left(\int_A \sigma_{xx}^{0}dA\right)\dot{\varepsilon}_{xx}dx - \int_L\left(\int_A \sigma_{xx}^{1}dA\right)\dot{\varepsilon}_{xx}^{\nabla}dx = 0. \quad (5)$$

In Equation (5), the following sectional axial-force contributions can be defined:

$$N(x) = \int_A \sigma_{xx}dA\,; N_0(x) = \int_A \sigma_{xx}^{0}dA,$$
$$N_1(x) = \int_A \sigma_{xx}^{1}dA, \quad (6)$$

where $N(x)$, $N_0(x)$, and $N_1(x)$ represent the sectional axial forces associated, respectively, with the nonlocal axial stress σ_{xx}, the local axial stress σ_{xx}^{0}, and the higher-order axial stress σ_{xx}^{1}on the bar section.

With Equation (6), the thermodynamic condition of Equation (4) can be written as

$$\int_L N(x)\,\dot{\varepsilon}_{xx}\,dx - \int_L N_0(x)\,\dot{\varepsilon}_{xx}dx - \int_L N_1(x)\,\dot{\varepsilon}_{xx}^{\nabla}dx = 0. \quad (7)$$

Subsequently, Equation (7) will be used to reveal the governing differential equilibrium equation as well as the associated natural boundary conditions for a nanobar-elastic substrate system.

2.2. Surface Elasticity Theory. When the surface-to-bulk ratio becomes large like in the case of nano-sized structures, excessive energy corresponding to the surface atoms induces the so-called surface-energy effect and renders the nano-sized structures exhibiting the size-dependent phenomenon. To include the surface-energy effect on a nano-sized bar, the Gurtin-Murdoch continuum model [27, 28] is called for. In this nonclassical continuum model, the bar cross-section is considered to be formed by a solid core and an outer surface shell perfectly bonded to its core, as shown in Figure 1. Since only axial stress is of interest in the present work, the constitutive relations of the surface proposed by Gurtin and Murdoch [27, 28] can be degenerated as:

$$\tau_{xx}^{\mathrm{Sur}} - \tau_{0}^{\mathrm{Sur}} = E^{\mathrm{Sur}}\varepsilon_{xx}^{\mathrm{Sur}}, \quad (8)$$

with τ_{xx}^{Sur} being the axial component of the surface stress tensor, τ_{0}^{Sur} being the residual surface stress under unconstrained conditions which can be obtained via atomistic simulations [43], E^{Sur} being the surface elastic modulus, u_{xx}^{Sur} being the surface axial displacement, and $\varepsilon_{xx}^{\mathrm{Sur}} = \partial u_{xx}^{\mathrm{Sur}}/\partial x$ being the surface strain.

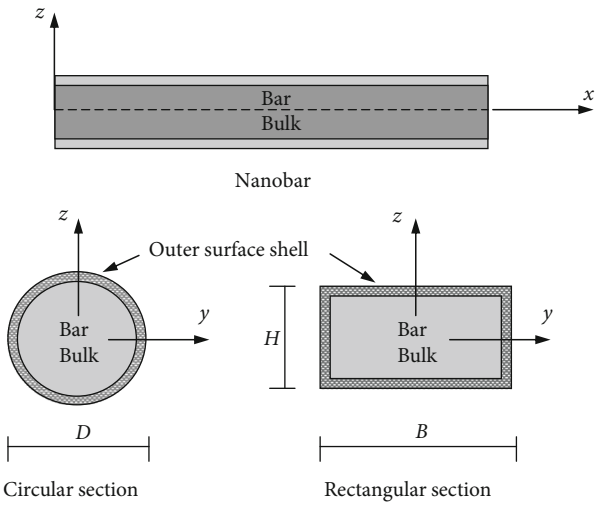

Figure 1: Nanobar with a surface layer.

3. Basic Equations of Nanobar-Elastic Substrate Systems

3.1. Compatibility Equations: Direct Approach. The bar-section strain $\varepsilon_{xx}(x)$, the bar-section strain gradient $\varepsilon^{\nabla}_{xx}(x)$, the surface strain $\varepsilon^{\mathrm{Sur}}_{xx}$, and the substrate deformation $\Delta_s(x)$ are the system section deformations and are related to the bar axial displacement $u_x(x)$ under the following compatibility conditions:

$$\varepsilon_{xx}(x) = \frac{\partial u_x(x)}{\partial x}, \qquad \varepsilon^{\nabla}_{xx}(x) = \frac{\partial \varepsilon_{xx}(x)}{\partial x} = \frac{\partial^2 u_x(x)}{\partial x^2}, \tag{9}$$

$$\varepsilon^{\mathrm{Sur}}_{xx}(x) = \frac{\partial u^{\mathrm{Sur}}_{xx}(x)}{\partial x} = \frac{\partial u_x(x)}{\partial x}, \tag{10}$$

$$\Delta_s(x) = u_x(x). \tag{11}$$

The bar-section compatibility conditions obey the infinitesimal strain assumption; the surface compatibility condition follows the assumption of a fully bonded condition between the solid core and an outer surface shell [44]; and the substrate compatibility condition conforms to the Winkler foundation hypothesis [45].

3.2. Differential Equilibrium Equation and Boundary Conditions: The Virtual Displacement Approach. Figure 2 shows a nanobar-elastic substrate system. Its governing differential equilibrium equation and its associated natural boundary conditions are consistently derived within the framework of the virtual displacement principle. To account for the nanobar-surrounding substrate interaction, the Winkler foundation model [45] is employed. The general form of the virtual displacement principle is expressed as

$$\delta W = \delta W_{\mathrm{int}} + \delta W_{\mathrm{ext}} = 0, \tag{12}$$

with δW being the system total virtual work, δW_{int} being the system internal virtual work, and δW_{ext} being the system external virtual work.

For the current system, δW_{int} and δW_{ext} are:

$$\begin{aligned}\delta W_{\mathrm{int}} = {} & \int_L \left(\int_A \sigma_{xx}(x) dA \right) \delta\varepsilon_{xx}(x)\, dx \\ & + \int_L \left(\oint_\Gamma \left(\tau^{\mathrm{Sur}}_{xx}(x) - \tau^{\mathrm{Sur}}_0 \right) d\Gamma \right) \delta\varepsilon^{\mathrm{Sur}}_{xx}(x) dx \\ & + \int_L D_s(x) \delta\Delta_s(x) dx,\end{aligned} \tag{13}$$

$$\delta W_{\mathrm{ext}} = -\int_L p_x(x) \delta u_x(x) dx - \delta \mathbf{U}^T \mathbf{P}, \tag{14}$$

where $D_s(x)$ represents the elastic substrate force, $\Delta_s(x)$ the elastic substrate deformation, and $p_x(x)$ the longitudinal distributed load. The vector $\mathbf{P} = \{ P_1 \quad P_2 \quad P_3 \quad P_4 \}^T$ collects forces acting at the bar ends, and the vector $\mathbf{U} = \{ U_1 \quad U_2 \quad U_3 \quad U_4 \}^T$ collects their conjugate-work displacements at the bar ends. It is noted that in Equation (13) the first, second, and third terms define, respectively, contributions of the bar-bulk material, of the surface layer, and of the surrounding elastic substrate to the system internal virtual work.

Recalling the stress resultant definition of Equation (6) and subsequently imposing the thermodynamics condition of Equation (7), Equation (13) becomes

$$\begin{aligned}\delta W_{\mathrm{int}} = {} & \int_L N_0(x) \delta\varepsilon_{xx}(x) dx + \int_L N_1(x) \delta\varepsilon^{\nabla}_{xx}(x) dx \\ & + \int_L N_{\mathrm{Sur}}(x) \delta\varepsilon^{\mathrm{Sur}}_{xx}(x) dx + \int_L D_s(x) \delta\Delta_s(x) dx,\end{aligned} \tag{15}$$

where $N_{\mathrm{Sur}}(x)$ is the sectional axial force associated with the surface stress and is defined as

$$N_{\mathrm{Sur}}(x) = \oint_\Gamma \left(\tau^{\mathrm{Sur}}_{xx}(x) - \tau^{\mathrm{Sur}}_0 \right) d\Gamma. \tag{16}$$

Imposing compatibility conditions of Equations (9), (10), and (11), Equation (15) can be expressed as

$$\begin{aligned}\delta W_{\mathrm{int}} = {} & \int_L N_0(x) \frac{\partial \delta u_x(x)}{\partial x} dx + \int_L N_1(x) \frac{\partial^2 \delta u_x(x)}{\partial x^2} dx \\ & + \int_L N_{\mathrm{Sur}}(x) \frac{\partial \delta u_x(x)}{\partial x} dx + \int_L D_s(x) \delta u_x(x) dx.\end{aligned} \tag{17}$$

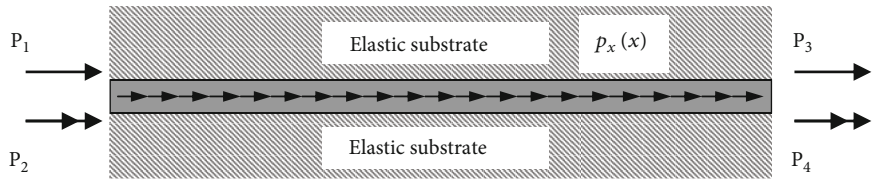

Figure 2: Nanobar-elastic substrate system under axial loads.

With Equations (14) and (17), Equation (12) can be expressed as

$$\delta W = \int_L N_0(x)\,\frac{\partial \delta u_x(x)}{\partial x}\,dx + \int_L N_1(x)\,\frac{\partial^2 \delta u_x(x)}{\partial x^2}\,dx + \int_L N_{Sur}(x)\,\frac{\partial \delta u_x(x)}{\partial x}\,dx + \int_L D_s(x)\delta u_x(x)dx - \int_L p_x(x)\delta u_x(x)dx - \delta \mathbf{U}^T \mathbf{P} = 0. \tag{18}$$

In order to move differential operators to all sectional stress resultants ($N_0(x)$, $N_1(x)$, and $N_{Sur}(x)$), integration by parts is imposed once on the first and third terms and twice on the second term of Equation (18), thus leading to the following expression:

$$\int_L \left(\frac{\partial^2 N_1(x)}{\partial x^2} - \frac{\partial N_0(x)}{\partial x} - \frac{\partial N_{\mathrm{Sur}}(x)}{\partial x} + D_s(x) - p_x(x)\right) \cdot \delta u_x(x)\,dx + \left[\left(N_0(x) + N_{\mathrm{Sur}}(x) - \frac{\partial N_1(x)}{\partial x}\right)\delta u_x(x)\right]_0^L + \left[N_1(x)\frac{\partial \delta u_x(x)}{\partial x}\right]_0^L - \delta \mathbf{U}^T \mathbf{P} = 0. \tag{19}$$

The boundary terms in Equation (19) show the nature of conjugate-work pairs between static and kinematic variables. The local-stress resultant $N_0(x)$, the surface stress resultant $N_{\mathrm{Sur}}(x)$, and the higher-order stress resultant gradient $\partial N_1(x)/\partial x$ are the conjugate-work pair of the axial displacement $u_x(x)$, while the higher-order stress resultant $N_1(x)$ is the conjugate-work pair of the axial-displacement gradient $\partial u_x(x)/\partial x$.

Following the Cartesian sign convention, Equation (19) can be expressed as

$$\int_L \left(\frac{\partial^2 N_1(x)}{\partial x^2} - \frac{\partial N_0(x)}{\partial x} - \frac{\partial N_{\mathrm{Sur}}(x)}{\partial x} + D_s(x) - p_x(x)\right) \cdot \delta u_x(x)\,dx - \delta U_1\left[\left(N_0(x) + N_{\mathrm{Sur}}(x) - \frac{\partial N_1(x)}{\partial x}\right)_{x=0} + P_1\right] - \delta U_2\left[(N_1(x))_{x=0} + P_2\right]_0^L + \delta U_3\left[\left(N_0(x) + N_{\mathrm{Sur}}(x) - \frac{\partial N_1(x)}{\partial x}\right)_{x=L} - P_3\right] + \delta U_4\left[(N_1(x))_{x=L} - P_4\right]_0^L = 0. \tag{20}$$

The following governing differential equilibrium equation of the nanobar-elastic substrate system can be obtained by accounting for arbitrariness of $\delta u_x(x)$:

$$\frac{\partial^2 N_1(x)}{\partial x^2} - \frac{\partial N_0(x)}{\partial x} - \frac{\partial N_{\mathrm{Sur}}(x)}{\partial x} + D_s(x) - p_x(x) = 0 : \text{for } x \in (0, L). \tag{21}$$

The following end-boundary force conditions (natural boundary conditions) can be gained by accounting for the arbitrariness of $\delta \mathbf{U}$:

$$P_1 = -\left(N_0(x) + N_{\mathrm{Sur}}(x) - \frac{\partial N_1(x)}{\partial x}\right)_{x=0}, \quad P_2 = -(N_1(x))_{x=0},$$
$$P_3 = \left(N_0(x) + N_{\mathrm{Sur}}(x) - \frac{\partial N_1(x)}{\partial x}\right)_{x=L}, \quad P_4 = (N_1(x))_{x=L}. \tag{22}$$

3.3. Sectional Constitutive Relations. In order to establish the sectional constitutive relations, Equations (3) and (8) are, respectively, substituted into Equations (6) and (16) and the compatibility conditions of Equations (9) and (10) are imposed, resulting in the following expression:

$$N_0(x) = E_{xx}A\,\frac{\partial u_x(x)}{\partial x},$$
$$N_1(x) = (E_{xx}A)(e_0 a)^2\,\frac{\partial^2 u_x(x)}{\partial x^2}, \tag{23}$$
$$N_{\mathrm{Sur}}(x) = E^{\mathrm{Sur}}\Gamma\,\frac{\partial u_x(x)}{\partial x},$$

where $A = \int_A dA$ being the section area and $\Gamma = \oint_\Gamma d\Gamma$ being the section perimeter.

Enforcing the compatibility condition of Equation (11), the constitutive relation of the elastic substrate medium becomes

$$D_s(x) = k_s u_x(x), \tag{24}$$

with k_s being the elastic substrate modulus.

A complete set of basic equations (compatibility conditions, equilibrium equation, and sectional constitutive relation) are presented together in the classical Tonti's diagram [46] as shown in Figure 3. A whole picture of the problem formulation can be seen from this diagram.

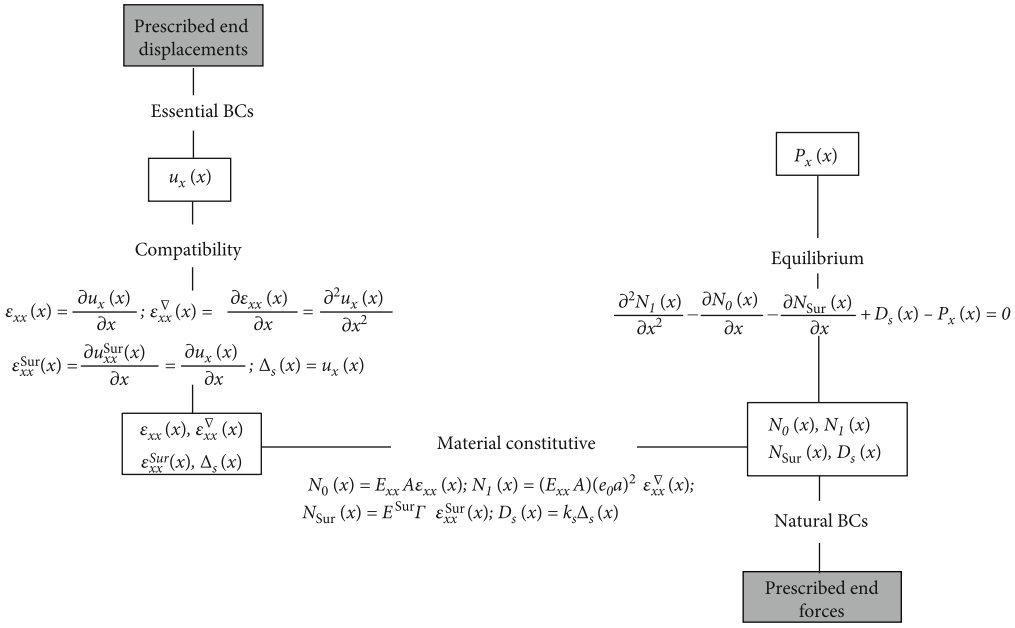

Figure 3: Tonti's diagram for nanobar-elastic substrate system: basic governing differential equations.

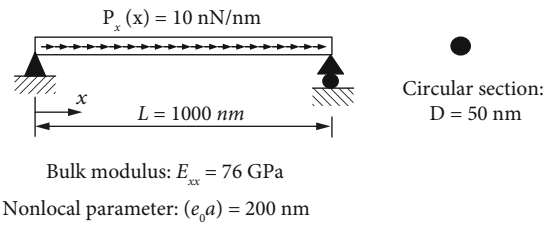

Figure 4: Circular section silver nanowire under uniformly distributed load for Simulation I.

3.4. Displacement Solution of Basic Equations. Within the framework of the displacement formulation, the solution to the problem is presented. The axial displacement $u_x(x)$ thus serves as the primary unknown. Substituting Equations (23) and (24) into Equation (21), the governing differential equilibrium equation can be written in terms of the axial displacement $u_x(x)$ as

$$(E_{xx}A)(e_0a)^2\frac{\partial^4 u_x(x)}{\partial x^4} - \left(E_{xx}A + E^{\mathrm{Sur}}\Gamma\right)\frac{\partial^2 u_x(x)}{\partial x^2} + k_s u_x(x) - p_x(x) = 0 : \text{for } x \in (0, L). \tag{25}$$

Equation (25) serves as a backbone equation to solve for the displacement solution of the problem and its higher order (4^{th} order) is associated with the strain gradient contribution to the bar-bulk material model. For the solution to Equation (25), both nonlocal and surface-energy effects influence the homogeneous part but play no role in dictating the particular part. It is worth mentioning that the governing differential equilibrium equation obtained for the nanobar-elastic substrate medium system proposed by Limkatanyu et al. [31] is of the 2^{nd} order, and both nonlocal and surface effects influence the homogeneous part while only nonlocal effect affects the particular part. When nonlocal and surface-energy effects are both ignored ($(e_0a) = E^{\mathrm{Sur}} = 0$), the differential equilibrium equation of a conventional (local) bar-elastic medium system is recovered. This degenerated form of Equation (25) finds a wide spectrum of applications in civil engineering problems, such as axially loaded piles [47] and reinforcing bars embedded in concrete [48].

To analytically determine the axial-displacement solution, both essential and natural boundary conditions are required. Special care is needed to handle the natural boundary conditions related to prescribed lower-order end force and/or higher-order end force. In other words, it is necessary to define both lower-order end force and higher-order end force in terms of the axial displacement $u_x(x)$. This can be accomplished by substituting Equation (23) into the end-boundary force conditions (natural boundary conditions) of Equation (22), resulting in the following expressions:

$$\begin{aligned}
P_1 &= -\left(\left(E_{xx}A + E^{\mathrm{Sur}}\Gamma\right)\frac{\partial u_x(x)}{\partial x} - (E_{xx}A)(e_0a)^2\frac{\partial^3 u_x(x)}{\partial x^3}\right)_{x=0},\\
P_2 &= -\left((E_{xx}A)(e_0a)^2\frac{\partial^2 u_x(x)}{\partial x^2}\right)_{x=0},\\
P_3 &= \left(\left(E_{xx}A + E^{\mathrm{Sur}}\Gamma\right)\frac{\partial u_x(x)}{\partial x} - (E_{xx}A)(e_0a)^2\frac{\partial^3 u_x(x)}{\partial x^3}\right)_{x=L},\\
P_4 &= \left((E_{xx}A)(e_0a)^2\frac{\partial^2 u_x(x)}{\partial x^2}\right)_{x=L}.
\end{aligned} \tag{26}$$

4. Numerical Simulations

The present work employs three numerical simulations to study the characteristics and behaviors of the proposed

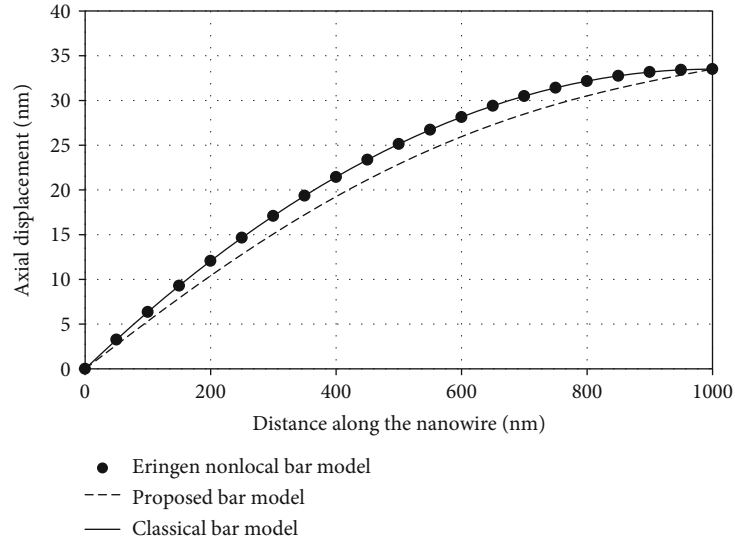

Figure 5: Nanowire axial displacement versus distance along the nanowire for Simulation I.

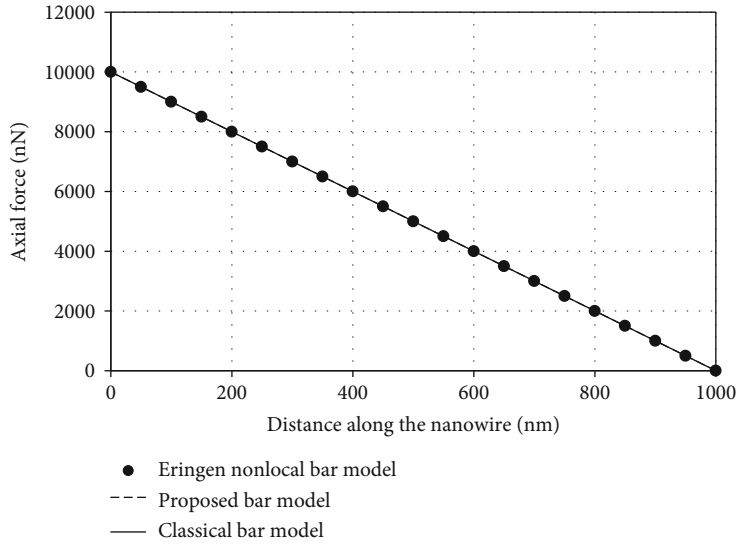

Figure 6: Nanowire axial force versus distance along the nanowire for Simulation I.

nanobar-elastic substrate model. The first considering only the small-scale effect is employed to present the capability of the proposed model in eliminating the paradoxical response associated with the Eringen nonlocal differential model; the second is employed to characterize the responses of the nanowire-elastic substrate system; and the third is employed to demonstrate the dependence of the system effective Young's modulus on several system parameters.

4.1. Simulation I: Eringen Nonlocal Bar Model vs. Thermodynamics-Based Strain Gradient Bar Model. The first simulation considers only the nanostructure-dependent effect of the bar-bulk material. Therefore, model parameters associated with surface-energy effect and the surrounding elastic substrate media are set to be zero ($E^{\text{Sur}} = 0$ and $k_s = 0$). A circular silver nanowire of Figure 4 is exerted by a uniformly distributed load $p_x(x)$ of 10 nN/nm. Geometric properties of the silver nanowire follow those employed by Juntarasaid et al. [20]. The span length L and diameter D of the silver nanowire are 1000 nm and 50 nm, respectively. As suggested by He and Lilley [49], the bulk modulus E_{xx} of the silver nanowire is 76 GPa. The nonlocal parameter $(e_0 a)$ of 200 nm follows the one used by Yang and Lim [50]. Three different bar models based on different constitutive models are employed to simulate the responses of the silver nanowire. The first one employs the local (conventional) model; the second, as proposed by Limkatanyu et al. [31], employs the Eringen differential nonlocal model; and the third, as proposed in the present work, employs the thermodynamics-based strain gradient model. To ease the model comparison, governing differential equilibrium equations and the boundary conditions for all bar models are summarized in Appendix I.

Figure 5 compares the axial-displacement distributions obtained from all bar models and shows that the axial-

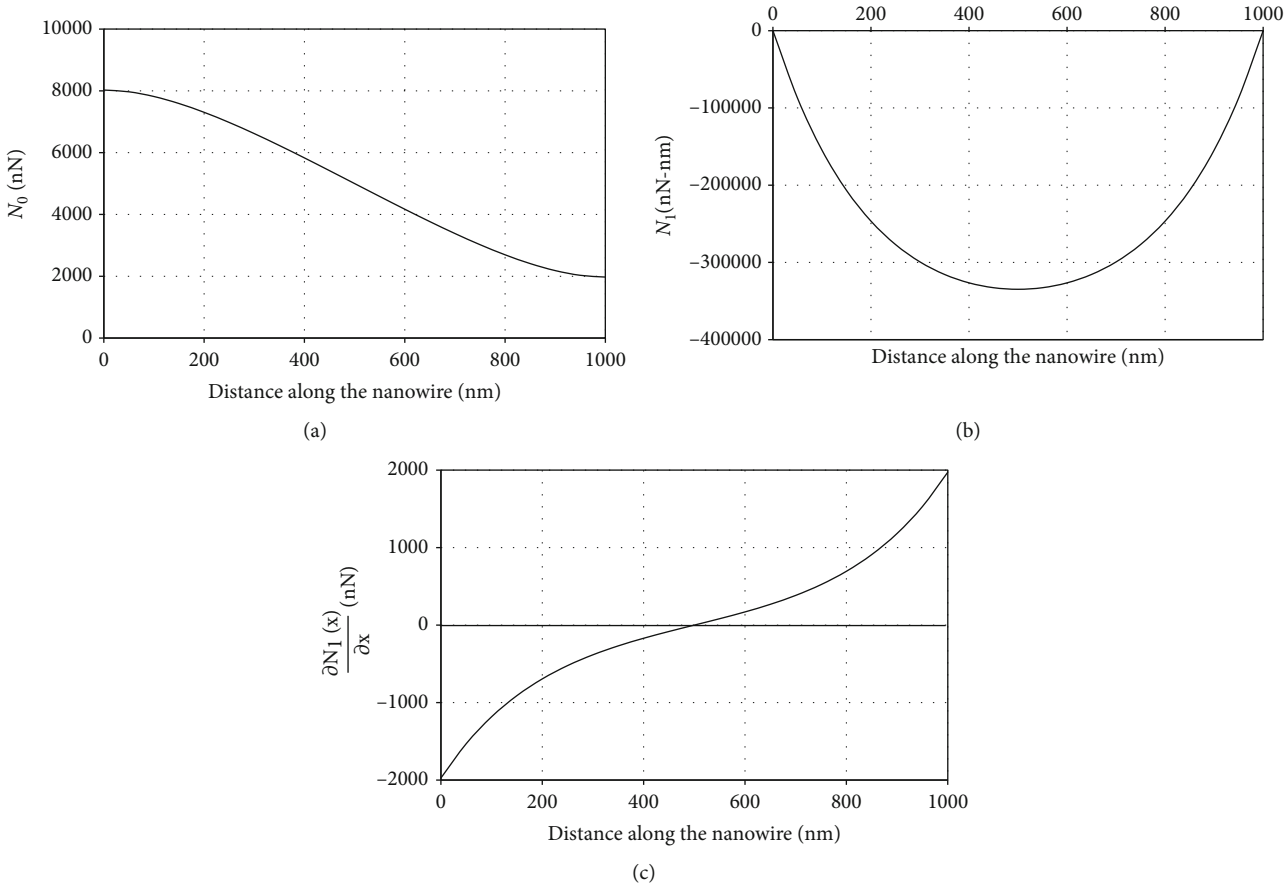

Figure 7: Axial-force responses versus distance along the nanowire for Simulation I. (a) Nanowire local axial force $N_0(x)$. (b) Nanowire higher-order axial force $N_1(x)$. (c) Nanowire higher-order axial-force gradient $\partial N_1(x)/\partial x$.

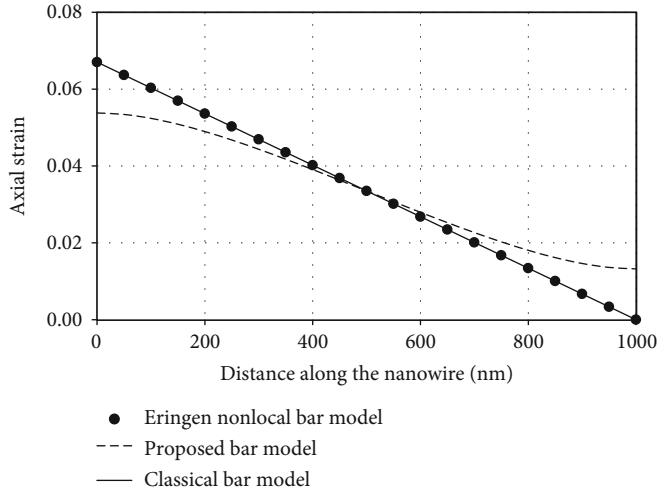

Figure 8: Nanowire axial strain versus distance along the nanowire for Simulation I.

displacement responses obtained from both the local bar model and Eringen nonlocal bar model are identical. In other words, the influence of nonlocality on the nanowire displaced shape is nullified for this particular case when subjected to a uniformly distributed load. Peddieson et al. [19] also noticed a similar observation in the case of a cantilever beam subjected to end force. In literatures, several researchers [51, 52] have considered this observation a paradox. Romano et al. [23] diagnosed this paradoxical result and indicated that adoption of Eringen nonlocal constitutive model caused the ill-posed condition, thus admitting no solution. More details regarding to this issue can be found in Romano et al. [23]. As shown in Figure 5, the thermodynamics-based strain gradient bar model proposed in this study shows no paradoxical

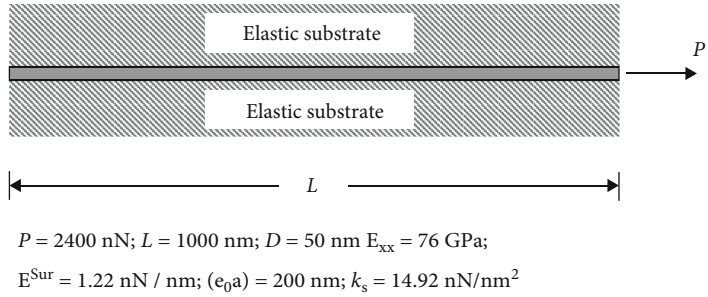

Figure 9: Free-free nanowire-elastic substrate system under an end force for Simulation II.

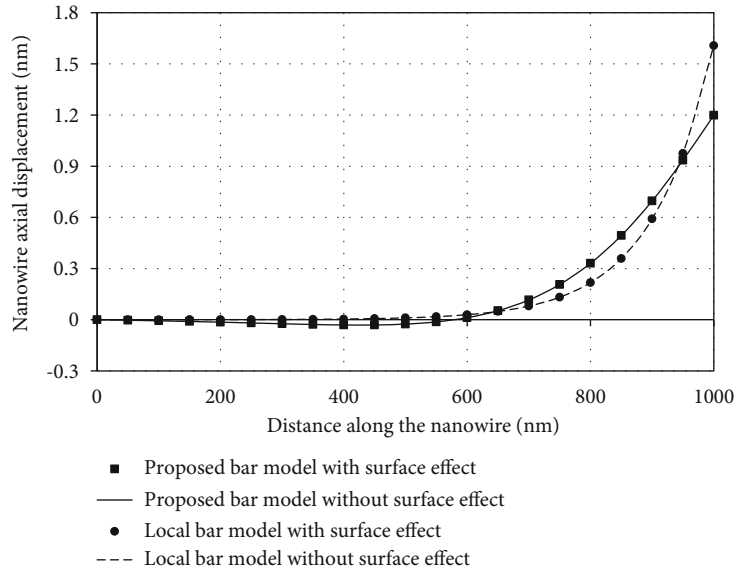

Figure 10: Nanowire axial displacement versus distance along the nanowire for Simulation II.

result and yields a stiffer axial-displacement response. This increased system stiffness associated with nanostructure effect conforms well to both analytical results and experimental evidences published in literatures [18, 25, 53].

Figure 6 presents the nanowire axial-force distributions obtained from all three bar models and indicates that the axial-force distributions obtained from all models are identical. In other words, the axial-force responses are not affected by bar-bulk material constitutive models. This attribute is related to the statically determinate nature of the simply supported bar system. It is worth noting that the axial-force distribution must be linear as required by the differential equilibrium equation. To further investigate the axial-force distribution nature of the proposed bar model, Figure 7 plots the distributions of local axial force $N_0(x)$, higher-order axial force $N_1(x)$, and higher-order axial-force gradient $\partial N_1(x)/\partial x$. Figure 7(a) shows the local axial-force distribution and clearly indicates that the local axial force $N_0(x)$ is not in equilibrium with a uniformly distributed load $p_x(x) = 10$ nN/nm and violates the force boundary condition at the right end. The higher-order axial-force distribution shown in Figure 7(b) confirms satisfaction of higher-order force boundary conditions at both bar ends ($N_1(0) = N_1(L) = 0$). Figure 7(c) shows the distribution of the higher-order axial-force gradient. It is worth remarking that in the proposed bar model, the axial force $N(x)$ is defined in terms of the local axial force $N_0(x)$ and the higher-order axial-force gradient $\partial N_1(x)/\partial x$ as dictated by the boundary term of Equation (22).

Figure 8 compares the axial-strain distributions obtained from all three bar models. Clearly, axial-strain distributions obtained from the local bar model and the Eringen nonlocal bar model are identical due to the aforementioned paradoxical displacement response and resemble the shape of axial-force distributions shown in Figure 5. However, the proposed bar model results in a different axial-strain distribution as characterized by the bar-bulk material constitutive model. It is also noted that the axial-strain distribution obtained with the proposed model resembles the shape of local axial-force distribution shown in Figure 7(a) as dictated by Equation (23).

4.2. Simulation II: Response of a Nanowire-Elastic Substrate System. As shown in Figure 9, the second simulation investigates the response of a free-free nanowire-elastic substrate system under an end force P of 2400 nN. The geometric and material properties of the nanowire follows those employed in Simulation I. The surface elastic modulus E^{Sur} of 1.22 nN/nm comes from that used by He and Lilley [49].

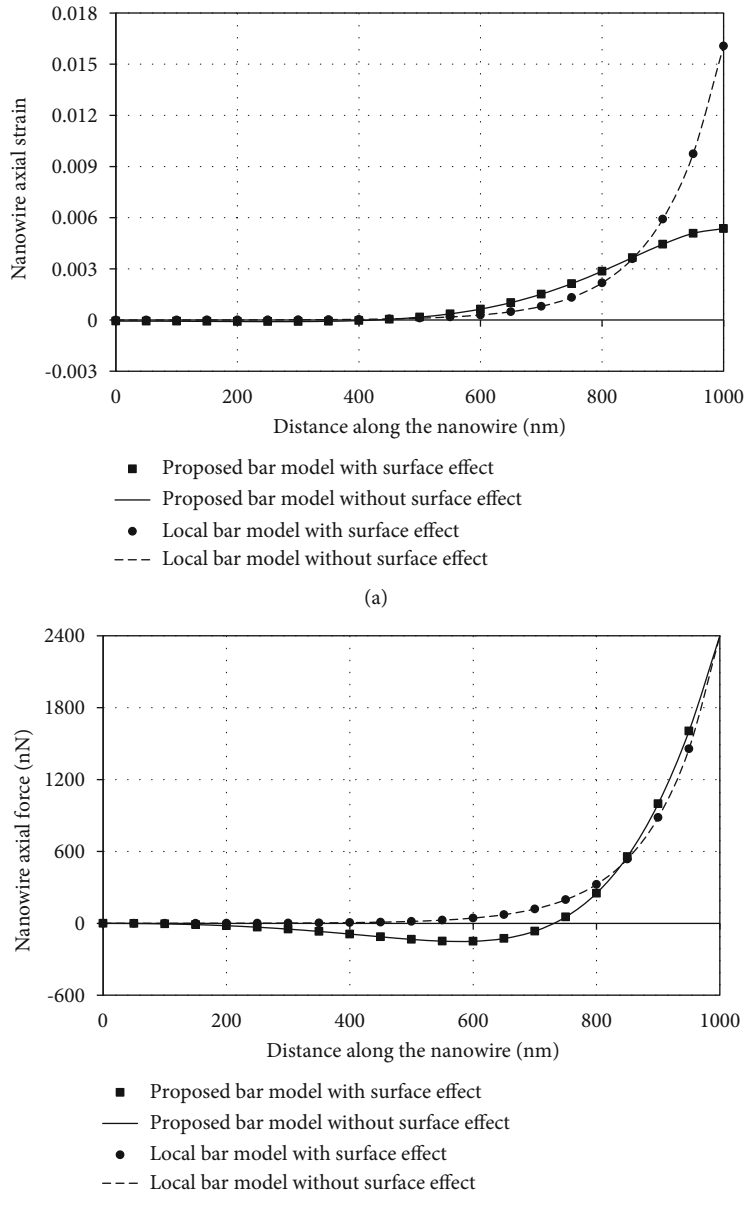

Figure 11: Nanowire axial strain (a) and nanowire axial force (b) versus distance along the nanowire for Simulation II.

For the substrate medium, a stiffness coefficient K_s of 95×10^{-3} nN/nm^3 is assumed, yielding an elastic substrate stiffness k_s of 14.92 nN/nm^2. This value for the substrate is suggested by Liew et al. [54] to represent the surrounding substrate medium as polymer. In this simulation, four analysis scenarios are investigated using the proposed nanobar-elastic substrate model. In the first two scenarios, the surface-energy effect on the nonlocal nanowire-elastic substrate responses is investigated while in the two remaining scenarios, the surface-energy effect on the local nanowire-elastic substrate responses is studied. Governing differential equilibrium equations and boundary conditions for all scenarios are summarized in Appendix II.

Figure 10 compares axial-displacement responses obtained from all the four scenarios. It is noted that for these specific values of system parameters, influences of the surface-energy effect are less pronounced than those of the nonlocal effect. Inclusion of the nonlocal effect results in a stiffer nanowire-elastic substrate system. When the nonlocal effect is taken into account, a larger portion of the nanowire is mobilized. It can also be observed that approximately half of the nonlocal nanowire-elastic substrate system is in the leftward (negative) direction while a whole portion of the local nanowire-elastic substrate system is in the rightward (positive) direction. This peculiar but unique displacement response is associated with the higher-order governing differential equation and the statical indeterminacy of the nanowire-elastic substrate system.

Figures 11(a) and 11(b) show the nanowire axial-strain and axial-force distributions obtained from the four analysis

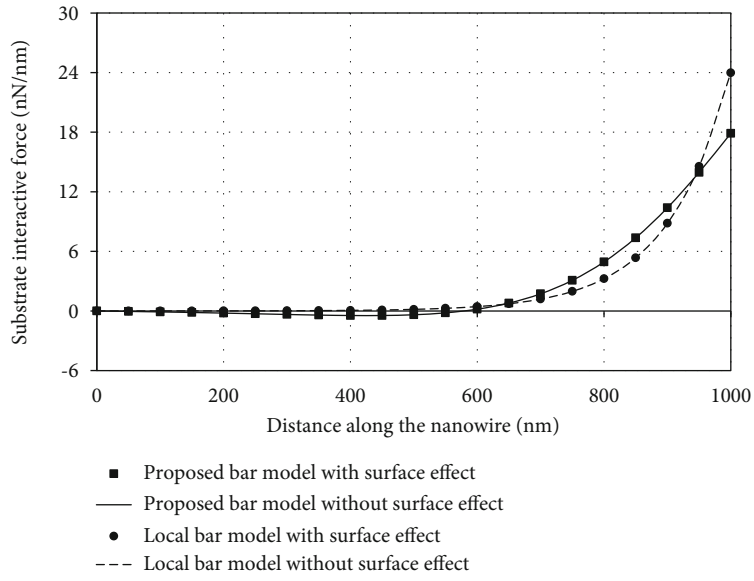

Figure 12: Substrate interactive force versus distance along the nanowire for Simulation II.

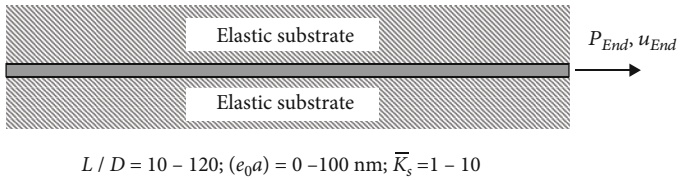

Figure 13: Schematic and values used in Simulation III.

scenarios, respectively. Like observations made on Figure 10, influences of the surface-energy effect are less noticeable than those of the nonlocal effect. It is observed from Figure 11(a) that the characteristics of axial-strain distributions obtained from the local bar model and the strain gradient bar model are drastically different at the far right end. The axial-strain distribution associated with the local model tends to be localized near the loading end while that associated with the strain gradient model appears to be spreading smoothly from the loading end. The maximum axial strain obtained with the local model is approximately three times larger than that obtained with the strain gradient model. The characteristics of axial-force distributions obtained from the local model and the strain gradient model are compared in Figure 11(b). The axial-force diagram obtained with the strain gradient model shows that a larger portion of the nanowire participates in the axial-force action. Furthermore, it also indicates that a large portion of the nanowire is in compression (negative value). This peculiar but unique axial-force response is associated with the higher-order governing differential equation and the statical indeterminacy of the nanowire-elastic substrate system.

Figure 12 shows the substrate interactive-force distributions obtained from the four scenarios. Following the Winkler foundation hypothesis, the shapes of the substrate interactive-force diagrams resemble those of the axial-displacement diagrams. Similar to the observation made in Figures 10 and 11, the nonlocal effect is more pronounced than the surface-energy effect in characterizing the substrate interactive-force diagram for these specific values of system parameters.

4.3. Simulation III: Parametric Studies of Nanowire-Elastic Substrate Systems. Simulation III is aimed at illustrating the size-dependent and nanostructure-dependent effects on the effective Young's modulus of the system through parametric studies of nanowire-elastic substrate systems shown in Figure 13. The surface elastic modulus E^{Sur} of 1.22 nN/nm is assumed. System parameters studied herein are the nonlocal parameter, the nanowire diameter, and the substrate stiffness. The nonlocal parameter $(e_0 a)$ varies from zero to 100 nm. The nanowire diameter parameter, defined through the slenderness ratio L/D, varies from 8.3 to 100 nm. Thus, the corresponding slenderness ratio L/D varies from 120 to 10. The following nondimensional substrate stiffness parameter $\bar{K}_s$ ranging from 1 to 10 is employed to define the substrate stiffness parameter K_s, thus

$$\bar{K}_s = \frac{K_s \Gamma L^2}{E_{xx} A}. \tag{27}$$

Adopting a similar approach suggested by He and Lilley [49], the so-called effective Young's modulus E_{xx}^{eff} can be computed as follows: First, the proposed model is used to compute the end displacement u_{End} of the nanowire-elastic

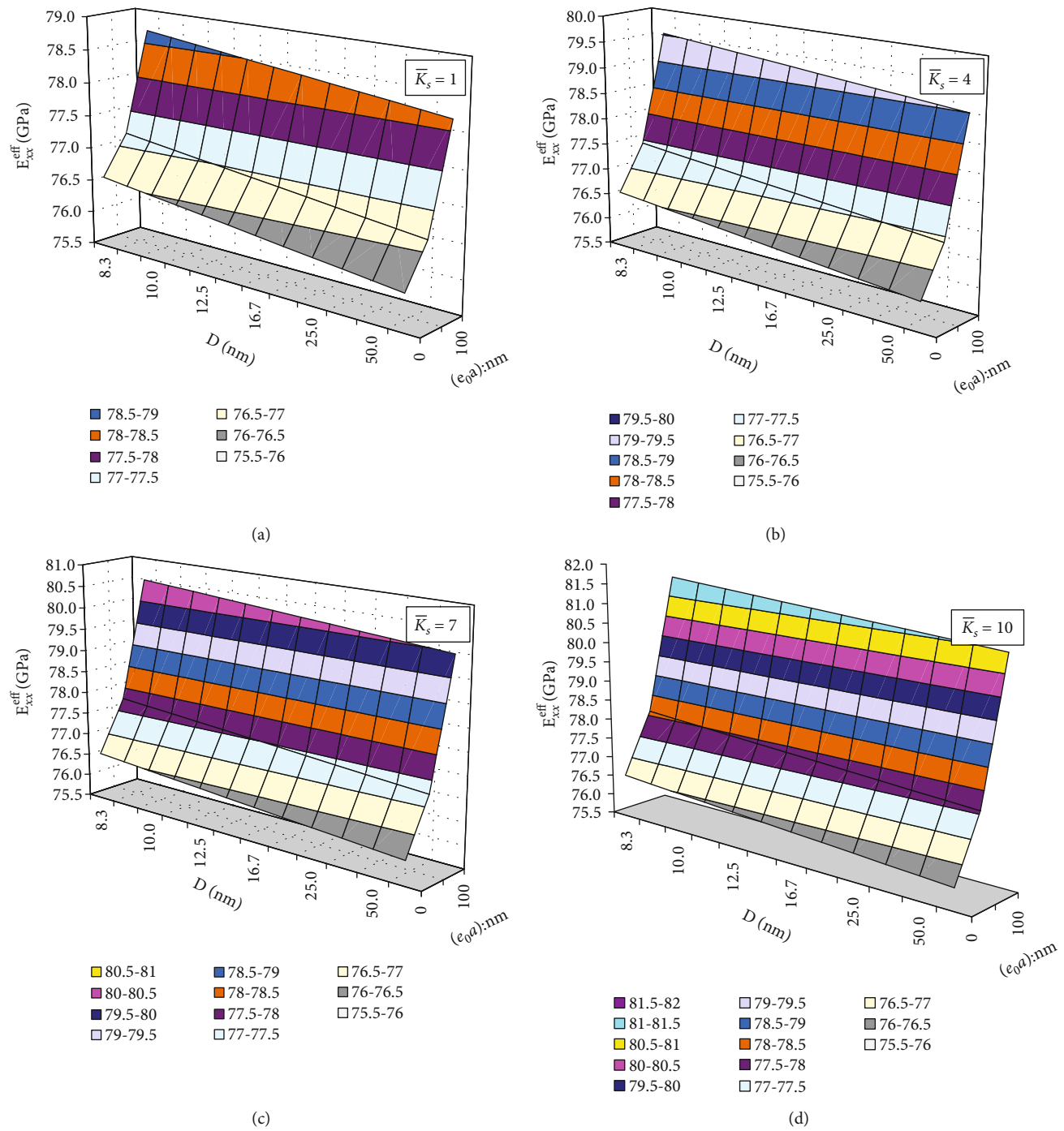

Figure 14: Variation of effective Young's modulus with nanowire diameter and nonlocal scale parameter for various elastic substrate stiffness nanowire for Simulation III.

substrate system. Then, E_{xx}^{eff} is computed by solving the following nonlinear relation:

$$u_{\text{End}} = \frac{P_{\text{End}} \coth\left(\sqrt{k_s/E_{xx}^{\text{eff}}AL}\right)}{\sqrt{k_s E_{xx}^{\text{eff}} A}}, \tag{28}$$

where the right-hand side of Equation (28) represents the end displacement analytically obtained from the classical bar model embedded in an elastic medium.

The variation of the effective Young's modulus E_{xx}^{eff} with the nonlocal parameter (e_0a) and diameter D is shown in Figures 14(a)–14(d) for nanowire-elastic substrate systems with, respectively, nondimensional substrate stiffness parameter $\bar{K}_s$ of 1, 4, 7, and 10. Generally, the effective Young's

modulus increases with increasing nonlocal parameter and decreasing nanowire diameter especially for larger values of nondimensional substrate stiffness parameters. Clearly, nonlocality, surface elasticity, and nanowire-surrounding substrate interaction are critical to the characterization of the size-dependent effect on the effective Young's modulus of the system. It is worth remarking that a more-slender nanowire (with decreasing diameter) increases the nanowire surface area/section area ratio, rendering the surface-energy effect more pronounced. Furthermore, it is noticed that when the nonlocality is ignored ($(e_0a) = 0$), variation of the effective Young's modulus E_{xx}^{eff} with diameter D is independent of the nondimensional substrate stiffness parameter $\bar{K}_s$. This neutralization of the substrate stiffness is due to the disappearance of the nonlocal scale parameter as observed in Equation (25).

5. Summary and Conclusions

A size-dependent bar-elastic substrate model considering small-scale and surface-energy effects is formulated in this paper to characterize axial responses of nanowire-elastic substrate systems under tensile loadings. The nanostructure-dependent effect of the bar-bulk material is taken into account through the thermodynamics-based strain gradient model while the surface energy-dependent size effect is considered using the Gurtin-Murdoch surface model. In a direct manner, system compatibility conditions are obtained while within the framework of the virtual displacement principle, the system equilibrium condition and the corresponding natural boundary conditions are consistently obtained. The system sectional force-deformation relations are established with inclusion of nonlocal and surface-energy effects. To investigate the characteristics and behaviors of the nanowire-elastic substrate system, three numerical simulations are performed.

The first simulation confirms that the thermodynamics-based strain gradient bar model can demonstrate the nonlocal effect even in the case of uniformly distributed loads as opposed to the Eringen nonlocal bar model. The paradoxical characteristic inherent to Eringen differential nonlocal constitutive model is thus absent from the proposed nanobar model. A stiffer axial-displacement response associated with nanostructure effect is obtained with the proposed nanobar model when compared with those obtained with local and Eringen nonlocal bar models.

The second simulation shows that both global and local responses of a nanowire-elastic substrate system are dictated by the effects of nonlocality and surface energy. A stiffer nanowire-elastic substrate system is noticed when the effects of nonlocality and surface energy are accounted for. Peculiar but unique response distributions along the nanowire length result, and they are associated with the higher-order governing differential equation and the statical indeterminacy of the nanowire-elastic substrate system.

The third simulation indicates that surrounding substrate stiffness, nonlocal parameter, and surface energy increase the size-dependent effect on the system effective Young's modulus. With the disappearance of the nonlocal scale parameter, the influence of surrounding substrate stiffness on the system effective Young's modulus is nullified.

Appendix

A. Governing Differential Equations and Boundary Conditions for All Bar Models in Simulation I

A.1. Eringen's Nonlocal Bar Model by Limkatanyu et al. [36]. Governing Differential Equation:

$$-(E_{xx}A)\frac{\partial^2 u_x(x)}{\partial x^2} = p_x(x) - (e_0a)^2\frac{\partial^2 p_x(x)}{\partial x^2} : \text{for } x \in (0, L). \tag{A.1}$$

Boundary Conditions:

$$u_x(0) = 0, \tag{A.2}$$

$$N(L) = \left((E_{xx}A)\frac{\partial u_x(x)}{\partial x}\right)\Bigg|_{x=L} = 0. \tag{A.3}$$

A.2. Classical (Local) Bar Model. Governing Differential Equation:

$$-(E_{xx}A)\frac{\partial^2 u_x(x)}{\partial x^2} = p_x(x): \text{for } x \in (0, L). \tag{A.4}$$

Boundary Conditions:

$$u_x(0) = 0, \tag{A.5}$$

$$N(L) = \left((E_{xx}A)\frac{\partial u_x(x)}{\partial x}\right)\Bigg|_{x=L} = 0. \tag{A.6}$$

A.3. Proposed Bar Model. Governing Differential Equation:

$$(E_{xx}A)(e_0a)^2\frac{\partial^4 u_x(x)}{\partial x^4} - (E_{xx}A)\frac{\partial^2 u_x(x)}{\partial x^2} = p_x(x): \text{for } x \in (0, L). \tag{A.7}$$

Boundary Conditions:

$$u_x(0) = 0, \tag{A.8}$$

$$N(L) = \left(\left(E_{xx}A + E^{\text{Sur}}\Gamma\right)\frac{\partial u_x(x)}{\partial x} - (E_{xx}A)(e_0a)^2\frac{\partial^3 u_x(x)}{\partial x^3}\right)\Bigg|_{x=L} = 0, \tag{A.9}$$

$$N_1(0) = \left((E_{xx}A)(e_0a)^2\frac{\partial^2 u_x(x)}{\partial x^2}\right)\Bigg|_{x=0} = 0, \tag{A.10}$$

$$N_1(L) = \left((E_{xx}A)(e_0a)^2\frac{\partial^2 u_x(x)}{\partial x^2}\right)\Bigg|_{x=L} = 0. \tag{A.11}$$

B. Governing Differential Equations and Boundary Conditions for Scenarios in Simulation II

B.1. Scenario I: Proposed (Nonlocal) Bar Model with Surface Effect. Governing Differential Equation:

$$(E_{xx}A)(e_0a)^2\frac{\partial^4 u_x(x)}{\partial x^4} - \left(E_{xx}A + E^{\mathrm{Sur}}\Gamma\right)\frac{\partial^2 u_x(x)}{\partial x^2} + k_s u_x(x) - p_x(x) = 0 : \text{for } x \in (0, L). \tag{B.1}$$

Boundary Conditions:

$$N(0) = \left(\left(E_{xx}A + E^{\mathrm{Sur}}\Gamma\right)\frac{\partial u_x(x)}{\partial x} - (E_{xx}A)(e_0a)^2\frac{\partial^3 u_x(x)}{\partial x^3}\right)\Bigg|_{x=0} = 0, \tag{B.2}$$

$$N(L) = \left(\left(E_{xx}A + E^{\mathrm{Sur}}\Gamma\right)\frac{\partial u_x(x)}{\partial x} - (E_{xx}A)(e_0a)^2\frac{\partial^3 u_x(x)}{\partial x^3}\right)\Bigg|_{x=L} = P, \tag{B.3}$$

$$N_1(0) = \left((E_{xx}A)(e_0a)^2\frac{\partial^2 u_x(x)}{\partial x^2}\right)\Bigg|_{x=0} = 0, \tag{B.4}$$

$$N_1(L) = \left((E_{xx}A)(e_0a)^2\frac{\partial^2 u_x(x)}{\partial x^2}\right)\Bigg|_{x=L} = 0. \tag{B.5}$$

B.2. Scenario II: Proposed (Nonlocal) Bar Model without Surface Effect. Governing Differential Equation:

$$(E_{xx}A)(e_0a)^2\frac{\partial^4 u_x(x)}{\partial x^4} - (E_{xx}A)\frac{\partial^2 u_x(x)}{\partial x^2} + k_s u_x(x) - p_x(x) = 0 : \text{for } x \in (0, L). \tag{B.6}$$

Boundary Conditions:

$$N(0) = \left((E_{xx}A)\frac{\partial u_x(x)}{\partial x} - (E_{xx}A)(e_0a)^2\frac{\partial^3 u_x(x)}{\partial x^3}\right)\Bigg|_{x=0} = 0, \tag{B.7}$$

$$N(L) = \left((E_{xx}A)\frac{\partial u_x(x)}{\partial x} - (E_{xx}A)(e_0a)^2\frac{\partial^3 u_x(x)}{\partial x^3}\right)\Bigg|_{x=L} = P, \tag{B.8}$$

$$N_1(0) = \left((E_{xx}A)(e_0a)^2\frac{\partial^2 u_x(x)}{\partial x^2}\right)\Bigg|_{x=0} = 0, \tag{B.9}$$

$$N_1(L) = \left((E_{xx}A)(e_0a)^2\frac{\partial^2 u_x(x)}{\partial x^2}\right)\Bigg|_{x=L} = 0. \tag{B.10}$$

B.3. Scenario III: Local Bar Model with Surface Effect. Governing Differential Equation:

$$-\left(E_{xx}A + E^{\mathrm{Sur}}\Gamma\right)\frac{\partial^2 u_x(x)}{\partial x^2} + k_s u_x(x) - p_x(x) = 0 : \text{for } x \in (0, L). \tag{B.11}$$

Boundary Conditions:

$$N(0) = \left(\left(E_{xx}A + E^{\mathrm{Sur}}\Gamma\right)\frac{\partial u_x(x)}{\partial x}\right)\Bigg|_{x=0} = 0, \tag{B.12}$$

$$N(L) = \left(\left(E_{xx}A + E^{\mathrm{Sur}}\Gamma\right)\frac{\partial u_x(x)}{\partial x}\right)\Bigg|_{x=L} = P. \tag{B.13}$$

B.4. Scenario IV: Local Bar Model without Surface Effect. Governing Differential Equation:

$$-(E_{xx}A)\frac{\partial^2 u_x(x)}{\partial x^2} + k_s u_x(x) - p_x(x) = 0 : \text{for } x \in (0, L). \tag{B.14}$$

Boundary Conditions:

$$N(0) = \left((E_{xx}A)\frac{\partial u_x(x)}{\partial x}\right)\Bigg|_{x=0} = 0, \qquad N(L) = \left((E_{xx}A)\frac{\partial u_x(x)}{\partial x}\right)\Bigg|_{x=L} = P. \tag{B.15}$$

Data Availability

Responses of Eringen nonlocal bar model shown in Figures 5, 6, and 8 were used to support this study and are available at DOI: 10.1155/2013/635428. These prior studies are cited at relevant places within the text as references [31].

Conflicts of Interest

The authors declare that they have no conflicts of interest.

Acknowledgments

This study was supported by the TRF Senior Research Scholar under Grant RTA 6280012. Any opinions expressed in this paper are those of the authors and do not reflect the views of the sponsoring agencies. Special thanks go to a senior lecturer Mr. Wiwat Sutiwipakorn for reviewing and correcting the English of this paper. In addition, the authors would also like to thank the anonymous reviewers for their valuable and constructive comments.

References

[1] H. G. Craighead, "Nanoelectromechanical systems," *Science*, vol. 290, no. 5496, pp. 1532–1536, 2000.

[2] F. Patolsky and C. M. Lieber, "Nanowire nanosensors," *Materials Today*, vol. 8, no. 4, pp. 20–28, 2005.

[3] X. L. Feng, R. He, P. Yang, and M. L. Roukes, "Very high frequency silicon nanowire electromechanical resonators," *Nano Letters*, vol. 7, no. 7, pp. 1953–1959, 2007.

[4] K. Jensen, K. Kim, and A. Zettl, "An atomic-resolution nanomechanical mass sensor," *Nature Nanotechnology*, vol. 3, no. 9, pp. 533–537, 2008.

[5] S. Narendar and S. Gopalakrishnan, "Ultrasonic wave characteristics of nanorods via nonlocal strain gradient models," *Journal of Applied Physics*, vol. 107, no. 8, article 084312, 2010.

[6] K. Tapio, D. Shao, S. Auer et al., "A DNA-nanoparticle actuator enabling optical monitoring of nanoscale movements induced by an electric field," *Nanoscale*, vol. 10, no. 41, pp. 19297–19309, 2018.

[7] B. Bhushan, *Springer Handbook of Nanotechnology: 3rd Edition*, Springer, New York, 2010.

[8] C. Z. Wang and K. M. Ho, "Tight-binding molecular dynamics for materials simulations," *Journal of Computer-Aided Materials Design*, vol. 3, no. 1-3, pp. 139–148, 1996.

[9] B. I. Yakobson, C. J. Brabec, and J. Bernholc, "Nanomechanics of carbon tubes: instabilities beyond linear response," *Physical Review Letters*, vol. 76, no. 14, pp. 2511–2514, 1996.

[10] L. J. D. Frink, A. G. Salinger, M. P. Sears, J. D. Weinhold, and A. L. Frischknecht, "Numerical challenges in the application of density functional theory to biology and nanotechnology," *Journal of Physics Condensed Matter*, vol. 14, no. 46, pp. 12167–12187, 2002.

[11] S. Cuenot, C. Frétigny, S. Demoustier-Champagne, and B. Nysten, "Surface tension effect on the mechanical properties of nanomaterials measured by atomic force microscopy," *Physical Review B*, vol. 69, no. 16, 2004.

[12] L. Wang and H. Hu, "Flexural wave propagation in single-walled carbon nanotubes," *Physical Review B*, vol. 71, no. 19, article 195412, 2005.

[13] G. Y. Jing, H. L. Duan, X. M. Sun et al., "Surface effects on elastic properties of silver nanowires: contact atomic-force microscopy," *Physical Review B*, vol. 73, no. 23, article 235409, 2006.

[14] R. D. Mindlin and H. F. Tiersten, "Effects of couple-stresses in linear elasticity," *Archive for Rational Mechanics and Analysis*, vol. 11, no. 1, pp. 415–448, 1962.

[15] A. C. Eringen, "Nonlocal polar elastic continua," *International Journal of Engineering Science*, vol. 10, no. 1, pp. 1–16, 1972.

[16] A. C. Eringen, "On differential equations of nonlocal elasticity and solutions of screw dislocation and surface waves," *Journal of Applied Physics*, vol. 54, no. 9, pp. 4703–4710, 1983.

[17] F. Yang, A. C. M. Chong, D. C. C. Lam, and P. Tong, "Couple stress based strain gradient theory for elasticity," *International Journal of Solids and Structures*, vol. 39, no. 10, pp. 2731–2743, 2002.

[18] D. C. C. Lam, F. Yang, A. C. M. Chong, J. Wang, and P. Tong, "Experiments and theory in strain gradient elasticity," *Journal of the Mechanics and Physics of Solids*, vol. 51, no. 8, pp. 1477–1508, 2003.

[19] J. Peddieson, G. R. Buchanan, and R. P. McNitt, "Application of nonlocal continuum models to nanotechnology," *International Journal of Engineering Science*, vol. 41, no. 3-5, pp. 305–312, 2003.

[20] C. Juntarasaid, T. Pulngern, and S. Chucheepsakul, "Bending and buckling of nanowires including the effects of surface stress and nonlocal elasticity," *Physica E: Low-dimensional Systems and Nanostructures*, vol. 46, pp. 68–76, 2012.

[21] M. A. Eltaher, M. E. Khater, S. Park, E. Abdel-Rahman, and M. Yavuz, "On the static stability of nonlocal nanobeams using higher-order beam theories," *Advances in Nano Research*, vol. 4, no. 1, pp. 51–64, 2016.

[22] S. Limkatanyu, W. Sae-Long, S. Horpibulsuk, W. Prachasaree, and N. Damrongwiriyanupap, "Flexural responses of nanobeams with coupled effects of nonlocality and surface energy," *ZAMM - Journal of Applied Mathematics and Mechanics/-Zeitschrift für Angewandte Mathematik und Mechanik*, vol. 98, no. 10, pp. 1771–1793, 2018.

[23] G. Romano, R. Barretta, M. Diaco, and F. Marotti de Sciarra, "Constitutive boundary conditions and paradoxes in nonlocal elastic nanobeams," *International Journal of Mechanical Sciences*, vol. 121, pp. 151–156, 2017.

[24] G. Romano and R. Barretta, "Nonlocal elasticity in nanobeams: the stress-driven integral model," *International Journal of Engineering Science*, vol. 115, pp. 14–27, 2017.

[25] R. Barretta and F. Marotti de Sciarra, "A nonlocal model for carbon nanotubes under axial loads," *Advances in Materials Science and Engineering*, vol. 2013, Article ID 360935, 6 pages, 2013.

[26] R. Barretta and F. Marotti de Sciarra, "Constitutive boundary conditions for nonlocal strain gradient elastic nano- beams," *International Journal of Engineering Science*, vol. 130, pp. 187–198, 2018.

[27] M. E. Gurtin and A. Ian Murdoch, "A continuum theory of elastic material surfaces," *Archive for Rational Mechanics and Analysis*, vol. 57, no. 4, pp. 291–323, 1975.

[28] M. E. Gurtin and A. Ian Murdoch, "Surface stress in solids," *International Journal of Solids and Structures*, vol. 14, no. 6, pp. 431–440, 1978.

[29] P. Lu, L. H. He, H. P. Lee, and C. Lu, "Thin plate theory including surface effects," *International Journal of Solids and Structures*, vol. 43, no. 16, pp. 4631–4647, 2006.

[30] F. F. Mahmoud, M. A. Eltaher, A. E. Alshorbagy, and E. I. Meletis, "Static analysis of nanobeams including surface effects by nonlocal finite element," *Journal of Mechanical Science and Technology*, vol. 26, no. 11, pp. 3555–3563, 2012.

[31] S. Limkatanyu, N. Damrongwiriyanupap, W. Prachasaree, and W. Sae-Long, "Modeling of Axially Loaded Nanowires Embedded in Elastic Substrate Media with Inclusion of Nonlocal and Surface Effects," *Journal of Nanomaterials*, vol. 2013, Article ID 635428, 14 pages, 2013.

[32] X. L. Gao and F. F. Mahmoud, "A new Bernoulli-Euler beam model incorporating microstructure and surface energy effects," *Zeitschrift für Angewandte Mathematik und Physik*, vol. 65, no. 2, pp. 393–404, 2014.

[33] S. Limkatanyu, P. Ponbunyanon, W. Prachasaree, K. Kuntiyawichai, and M. Kwon, "Correlation between beam on Winkler-Pasternak foundation and beam on elastic substrate medium with inclusion of microstructure and surface effects," *Journal of Mechanical Science and Technology*, vol. 28, no. 9, pp. 3653–3665, 2014.

[34] Y. Cui, Z. Zhong, D. Wang, W. U. Wang, and C. M. Lieber, "High performance silicon nanowire field effect transistors," *Nano Letters*, vol. 3, no. 2, pp. 149–152, 2003.

[35] Z. L. Wang and J. Song, "Piezoelectric nanogenerators based on zinc oxide nanowire arrays," *Science*, vol. 312, no. 5771, pp. 242–246, 2006.

[36] A. Khajeansari, G. H. Baradaran, and J. Yvonnet, "An explicit solution for bending of nanowires lying on Winkler–Pasternak elastic substrate medium based on the Euler–Bernoulli beam

theory," *International Journal of Engineering Science*, vol. 52, pp. 115–128, 2012.

[37] T. Zhao, J. Luo, and Z. Xiao, "Buckling analysis of a nanowire lying on Winkler–Pasternak elastic foundation," *Mechanics of Advanced Materials and Structures*, vol. 22, no. 5, pp. 394–401, 2014.

[38] P. Malekzadeh and M. Shojaee, "Surface and nonlocal effects on the nonlinear free vibration of non-uniform nanobeams," *Composites Part B: Engineering*, vol. 52, pp. 84–92, 2013.

[39] S. Limkatanyu, W. Prachasaree, N. Damrongwiriyanupap, and M. Kwon, "Exact stiffness matrix for nonlocal bars embedded in elastic foundation media: the virtual-force approach," *Journal of Engineering Mathematics*, vol. 89, no. 1, pp. 163–176, 2014.

[40] L. Lu, X. Guo, and J. Zhao, "A unified nonlocal strain gradient model for nanobeams and the importance of higher order terms," *International Journal of Engineering Science*, vol. 119, pp. 265–277, 2017.

[41] R. D. Mindlin, "On the equations of elastic materials with micro-structure," *International Journal of Solids and Structures*, vol. 1, no. 1, pp. 73–78, 1965.

[42] B. S. Altan and E. C. Aifantis, "On some aspects in the special theory of gradient elasticity," *Journal of the Mechanical Behavior of Materials*, vol. 8, no. 3, pp. 231–282, 1997.

[43] R. E. Miller and V. B. Shenoy, "Size-dependent elastic properties of nanosized structural elements," *Nanotechnology*, vol. 11, no. 3, pp. 139–147, 2000.

[44] R. C. Cammarata, "Surface and interface stress effects in thin films," *Progress in Surface Science*, vol. 46, no. 1, pp. 1–38, 1994.

[45] E. Winkler, *Die Lehre von der und Festigkeit*, Dominicus, Prag, 1867.

[46] E. Tonti, "The reason for analogies between physical theories," *Applied Mathematical Modelling*, vol. 1, no. 1, pp. 37–50, 1976.

[47] C. Buachart, C. Hansapinyo, and W. Kanok-Nukulchai, "Analysis of axial loaded pile in multilayered soil using nodal exact finite element model," *International Journal of GEOMATE*, vol. 14, no. 44, pp. 1–7, 2018.

[48] M. R. Salari and E. Spacone, "Finite element formulations of one-dimensional elements with bond-slip," *Engineering Structures*, vol. 23, no. 7, pp. 815–826, 2001.

[49] J. He and C. M. Lilley, "Surface effect on the elastic behavior of static bending nanowires," *Nano Letters*, vol. 8, no. 7, pp. 1798–1802, 2008.

[50] Y. Yang and C. W. Lim, "Non-classical stiffness strengthening size effects for free vibration of a nonlocal nanostructure," *International Journal of Mechanical Sciences*, vol. 54, no. 1, pp. 57–68, 2012.

[51] N. Challamel and C. M. Wang, "The small length scale effect for a non-local cantilever beam: a paradox solved," *Nanotechnology*, vol. 19, no. 34, article 345703, 2008.

[52] C. W. Lim, "On the truth of nanoscale for nanobeams based on nonlocal elastic stress field theory: equilibrium, governing equation and static deflection," *Applied Mathematics and Mechanics*, vol. 31, no. 1, pp. 37–54, 2010.

[53] W. D. Nix and H. Gao, "Indentation size effects in crystalline materials: a law for strain gradient plasticity," *Journal of the Mechanics and Physics of Solids*, vol. 46, no. 3, pp. 411–425, 1998.

[54] K. M. Liew, X. Q. He, and S. Kitipornchai, "Predicting nanovibration of multi-layered graphene sheets embedded in an elastic matrix," *Acta Materialia*, vol. 54, no. 16, pp. 4229–4236, 2006.